

螺芴对含三齿磷配体的铱配合物光电性能的影响

陈 熉¹ 王 月¹ 周跃跃¹ 王 平¹ 童碧海^{*,1} 冯敏强^{*,2} 王 松^{*,3}

(¹ 安徽工业大学冶金工程学院, 分子工程与应用化学研究中心,
冶金减排与资源综合利用教育部重点实验室, 马鞍山 243002)

(² 苏州大学功能纳米与软物质研究院, 苏州大学纳米协同创新中心,
江苏省碳基功能材料重点实验室, 苏州 215123)

(³ 湖北文理学院, 湖北省低维光电材料与器件重点实验室, 襄阳 441053)

摘要: 合成了一种含 4,5-二氮-9,9-螺二芴(sb)配体的三齿磷铱配合物 Ir(tpit)(sb)Cl(tpitH₂=亚磷酸三苯基酯), 通过核磁共振氢谱和磷谱及高分辨质谱对其结构进行了确定。X 射线单晶衍射分析表明, sb 配体的存在扭曲了分子结构, 有助于降低分子聚集及发光淬灭。与存在分子内 π - π 堆积的模型配合物 Ir(tpit)(bpy)Cl(bpy=2,2'-联吡啶)对比进行了光电性能的研究。结果表明在聚甲基丙烯酸甲酯(质量分数 1%)中配合物 Ir(tpit)(sb)Cl 的发光波长为 512 nm, 相对配合物 Ir(tpit)(bpy)Cl 的波长(520 nm)有了 8 nm 蓝移。配合物 Ir(tpit)(sb)Cl 的发光量子效率为 30%, 与配合物 Ir(tpit)(bpy)Cl 的 94%相比有明显降低, 说明了分子内 π - π 堆积作用在降低柔性基团非辐射跃迁率方面的重要作用。基于配合物 Ir(tpit)(sb)Cl 的有机电致发光器件, 最大电流效率和外量子效率分别为 14 cd·A⁻¹ 和 4.5%。而由于分子内 π - π 堆积作用, 基于配合物 Ir(tpit)(bpy)Cl 器件的最大电流效率和外量子效率分别高达 60 cd·A⁻¹ 和 18.2%。

关键词: 环金属铱(III)配合物; 三齿磷配体; 有机电致发光; 磷光; 螺芴

中图分类号: O614.82+5 文献标识码: A 文章编号: 1001-4861(2020)03-0494-09

DOI: 10.11862/CJIC.2020.045

Influence of Spirofluorene on Photoelectric Properties of Iridium Complexes Containing Tridentate Phosphite Ligands

CHEN Man¹ WANG Yue¹ ZHOU Yue-Yue¹ WANG Ping¹

TONG Bi-Hai^{*,1} FUNG Man-Keung^{*,2} WANG Song^{*,3}

(¹Key Laboratory of Metallurgical Emission Reduction & Resources Recycling, Ministry of Education,
Institute of Molecular Engineering and Applied Chemistry, School of Metallurgical Engineering,
Anhui University of Technology, Maanshan, Anhui 243002, China)

(²Jiangsu Key Laboratory for Carbon-Based Functional Materials & Devices, Institute of Functional Nano & Soft Materials (FUNSOM)
& Collaborative Innovation Center of Suzhou Nano Science and Technology, Soochow University, Suzhou, Jiangsu 215123, China)

(³Hubei Key Laboratory of Low Dimensional Optoelectronic Materials and Devices,
Hubei University of Arts and Science, Xiangyang, Hubei 441053, China)

Abstract: A cyclometalated iridium(III) complex Ir(tpit)(sb)Cl (tpitH₂=triphenyl phosphite) containing 4,5-diazo-9,9-spirobifluorene (sb) ligand was successfully synthesized and characterized by NMR spectroscopy and high resolution mass spectrometry. X-ray single crystal diffraction analysis showed that the existence of sb ligand distorted the structure of complex, which is beneficial for reducing the molecular aggregation and luminescent quenching. The photoelectric properties of complex Ir(tpit)(sb)Cl has been studied in comparison with those of the

收稿日期: 2019-05-30。收修改稿日期: 2019-12-03。

国家自然科学基金(No.21572001)资助项目。

*通信联系人。E-mail: tongbihai@163.com, mkfung@suda.edu.cn, wangsong1984@126.com

model complex Ir(tpit)(bpy)Cl (bpy=2,2'-bipyridine) existing intramolecular π - π stacking. The results show that the luminescence wavelength of complex Ir(tpit)(sb)Cl in polymethyl methacrylate (mass fraction 1%) was 512 nm, and had a blue shift of 8 nm compared to that of complex Ir(tpit)(bpy)Cl (520 nm). The quantum efficiency of the complex Ir (tpit)(sb)Cl was 30%, which is significantly lower than that of the complex Ir (tpit)(bpy)Cl (94%), indicating the radiative transition rate is reduced by spirofluorene. Based on the complex Ir (tpit)(sb)Cl, the maximum current efficiency and external quantum efficiency of OLED device are 14 $\text{cd} \cdot \text{A}^{-1}$ and 4.5%, respectively. The maximum current efficiency and external quantum efficiency of Ir(tpit)(bpy)Cl-based device are up to 60 $\text{cd} \cdot \text{A}^{-1}$ and 18.2%, respectively. CCDC: 1812631.

Keywords: cyclometalated iridium(III) complex; tridentate phosphite ligand; organic electroluminescence; phosphorescence; spirofluorene

0 Introduction

Organic light emitting diodes (OLEDs) are known as “Dream Display” owing to their several advantages, such as low energy consumption, spontaneous luminescence, which is expected to be the next generation panel display and solid-state lighting technique^[1-2]. Iridium complexes are widely used in OLEDs because of their high luminescent quantum efficiency^[3]. In order to meet the requirement of practicability, in addition to the luminescent efficiency, the long-term stability of devices greatly attracts the attention of researchers. In addition, exploring multidentate complexes with strong stability is the main topic of research today. For example, Chi et al.^[4] developed a collection of bis-tridentate Ir(III) metal complexes. In terms of these complexes, 100% of internal quantum efficiency was achieved, the entire visible region was covered, and the stability of the organic electroluminescent device was greatly increased. They also developed a class of facial tridentate phosphor neutral iridium complexes^[5-7], and the bis-cyclometallated phosphorus ligands were not luminescent because of broken conjugate and the dominant emissive groups were diimine ligands, which was rare in iridium complexes. At the same time, the intramolecular π - π accumulation in these complexes was also found, but the model complex Ir(tpit)(bpy)Cl was less studied and the solid state lighting as well as electroluminescence performance hadn't been reported. Our research group improved this kind of complexes with dipyrindine

ligands containing ester groups, the luminescence in solid state could be enhanced by 17 times compared with that in the solution state, which was caused by strong aggregation-induced luminescence enhancement effect^[8]. In addition, it was found that this kind of complexes can be used as silver ion probes with the detection limit up to 0.13 $\mu\text{mol} \cdot \text{L}^{-1}$ ^[9], indicating a good application prospect for these complexes. The stability of the iridium complexes was able to be enhanced by intramolecular π - π stacking. The most reported complexes with intramolecular π - π stacking were ionic, like which Chen et al.^[10] synthesized an ionic iridium complex containing intramolecular π - π accumulation. However, neutral complexes with intramolecular π - π stacking were rarely reported^[11-14]. For example, Congrave et al.^[15] synthesized some neutral complexes with phenylpyridine (ppy)-based cyclometalating ligands. The intramolecular π - π interaction weakens the elongation of excited state for metal-ligand, thus reduces the ability of external substances to enter the metal coordination center. The lifetime of electrochemical cells containing these iridium complexes could last up to 585 minutes, 4 times longer than that of materials without π - π interaction.

4,5-diazo-9,9-spirobifluorene (sb) is widely used in the transition metal complexes^[16-19], which is a kind of rigid diimine ligand^[20-21] and fluorene groups are linked to dipyrindine using carbon atoms with small conjugation, reducing the molecular aggregation and luminescent quenching in light-emitting iridium

complexes^[22-25]. For example, 22.6 and 26.2 $\text{lm} \cdot \text{W}^{-1}$ of luminous electrochemical cell power efficiency for complexes $[\text{Ir}(\text{ppy})_2\text{sb}]\text{PF}_6$ and $[\text{Ir}(\text{dFppy})_2\text{sb}]\text{PF}_6$ were achieved^[22], which were the highest efficiencies reported at the time. Since the ligand is electrically neutral, the iridium complexes prepared by it are ionic. Based on the above background, we synthesized neutral iridium complexes by introducing ligand sb (4,5-diazo-9,9-spirodifluorene) in tridentate phosphor. By comparing complex $\text{Ir}(\text{tpit})(\text{sb})\text{Cl}$ (tpitH_2 =triphenyl phosphite) with model complex $\text{Ir}(\text{tpit})(\text{bpy})\text{Cl}$ (bpy =2,2'-bipyridine) reported in the literature, the impact of diimine ligand on the performance of iridium complexes was studied.

1 Experimental

1.1 Materials and characterization

All reagents without special instructions are commercially analyzed pure products, which can be used directly after purchase. NMR were recorded on a BRUKER Avance III 400 spectrometer. X-ray crystallography diffraction data was tested by a Bruker SMART AEX II diffractometer. HRMS were determined by AB Triple TOF 5600^{plus} spectrometer. UV spectra were recorded on a TU-1901 spectrophotometer. Luminescence lifetime and quantum efficiency were measured by the Edinburgh (FLS-920) time-dependent single-photon counting fluorometer. Fluorescence spectra was obtained at room temperature using a PerkinElmer LS-55 spectrophotometer. Cyclic voltammetry was recorded in dichloromethane on a Chenhua CHI60A electrochemical workstation with the tetra-*n*-butyl amine hexafluorophosphate ($0.1 \text{ mol} \cdot \text{L}^{-1}$) as the supporting electrolyte, ferrocene as the external standard, glassy carbon electrode as the working electrode, platinum plate as the counter electrode, and saturated silver/silver chloride as the reference electrode. OLEDs were prepared by evaporation and film thickness was monitored by Inficon thickness measuring instrument with a resolution of $0.001 \text{ nm} \cdot \text{s}^{-1}$. Electroluminescence spectra, CIE coordinates, J - V characteristic curves, brightness and other parameters were measured by Photo Research

PR 670 photometer combining with Keithley 2400 dc power driver.

1.2 Syntheses of iridium complexes

$\text{Ir}(\text{tht})_3\text{Cl}_3$ (tht =tetrahydrothiophene)^[5], 4,5-diazo-9,9-spirodifluorene (sb)^[17] and reference Ir complex $\text{Ir}(\text{tpit})(\text{bpy})\text{Cl}$ (tpitH_2 =triphenyl phosphite, bpy =2,2'-bipyridine)^[6] were synthesized according to the literatures.

Synthesis of $\text{Ir}(\text{tpit})(\text{sb})\text{Cl}$: sb (0.29 g, 0.92 mmol), $\text{Ir}(\text{tht})_3\text{Cl}_3$ (0.52 g, 0.92 mmol), triphenyl phosphate (0.29 g, 0.92 mmol), sodium acetate (0.38 g, 4.6 mmol) and decalin (20 mL) were added in a 100 mL round-bottomed flask, and then the solution was heated for 12 h under nitrogen atmosphere. After the reaction was completed, the reaction mixture was cooled to room temperature, and then poured into the silica gel column. The decalin was eluted with petroleum ether, followed by elution with dichloromethane/ethyl acetate (3:1, V/V) to obtain the yellow solid of the complex $\text{Ir}(\text{tpit})(\text{sb})\text{Cl}$, with a yield of 53% (0.42 g). The crystals for single crystal diffraction were prepared by recrystallization with dichloromethane and *n*-hexane mixed solution. ^1H NMR (400 MHz, CDCl_3): δ 8.30 (d, J =8 Hz, 2H), 7.94 (d, J =8.1 Hz, 1H), 7.87 (d, J =7.7 Hz, 1H), 7.67 (d, J =5.9 Hz, 2H), 7.55 (t, J =8 Hz, 1H), 7.45 (t, J =8 Hz, 1H), 7.26~7.17 (m, 4H), 7.14~7.02 (m, 7H), 6.96~6.85 (m, 8H). ^{31}P NMR (162 MHz, CDCl_3): δ 113.35 (s, 1P). HRMS ((+)-ESI): m/z =819.139 0, Calcd. 819.138 9 for $[\text{C}_{41}\text{H}_{27}\text{IrN}_2\text{O}_3\text{P}][(\text{M}-\text{Cl})^+]$. Elemental analysis Calcd. For $\text{C}_{41}\text{H}_{27}\text{IrN}_2\text{O}_3\text{P}\text{Cl}$ (%): C 57.64, H 3.19, N 3.28. Found (%): C 57.62, H 3.20, N 3.27.

1.3 Structure determination

In order to study the structure of the complex, the single-crystal structure was also tested from dichloromethane solution at room temperature. A light yellow crystal of compound $\text{Ir}(\text{tpit})(\text{sb})\text{Cl}$ with approximate dimension of $0.25 \text{ mm} \times 0.23 \text{ mm} \times 0.20 \text{ mm}$ was selected, followed by mounted on a glass fiber. By using a Bruker SMART AEX II diffractometer equipped with a graphite-monochromator with Mo $K\alpha$ radiation ($\lambda=0.071\ 073 \text{ nm}$), the intensity data were collected with ω scan mode at 150(2) K. Intensity

data were obtained by empirical absorption. In the range of $2.243 < \theta < 24.997$ ($-11 \leq h \leq 15$, $-19 \leq k \leq 19$, $-22 \leq l \leq 22$), a total of 20 330 reflections were collected, of which 7 185 were independent ($R_{\text{int}}=0.048\ 2$) and 6 018 were observed with $I > 2\sigma(I)$. Based on the multi-scan technique, the intensity data were corrected for empirical absorption as well as for polarization and Lorentz effects^[26]. The structure was solved by direct method, and was optimized by full-matrix least-squares methods on F^2 with SHELX-97^[27].

By using fixed isotropic thermal parameters and riding model position parameters, the hydrogen atoms were located theoretically and refined. SQUEEZE was used in structural refinement to eliminate disordered solvent. By using anisotropic displacement parameters, all non-H atoms were refined. The refinement parameters and the crystal data of complex are shown in Table 1.

CCDC: 1812631.

Table 1 Crystal data, data collection and structure refinement parameters for complex Ir(tpit)(sb)Cl

Formula	$\text{C}_{42}\text{H}_{30}\text{Cl}_3\text{IrN}_2\text{O}_3\text{P}$	θ range for data collection / ($^\circ$)	2.243~24.997
Formula weight	939.07	$F(000)$	1 684
Crystal system	Orthorhombic	h, k, l	-11~15, -19~19, -22~22
Space group	$Pbca$	Reflection measured	20 330
a / nm	1.334 2(3)	Unique reflection	7 185
b / nm	1.651 9(4)	R_{int}	0.048 2
c / nm	1.874 6(5)	Parameter refined	443
V / nm ³	4.131 8(18)	R (F), wR (F^2)* (all reflections)	0.064 9, 0.069 7
Z	4	GOF (F^2)	0.92
D_c / (g·cm ⁻³)	1.375	Largest diff. peak and hole / (e·nm ⁻³)	756 and -521
$\mu(\text{Mo } K\alpha)$ / cm ⁻¹	6.2		

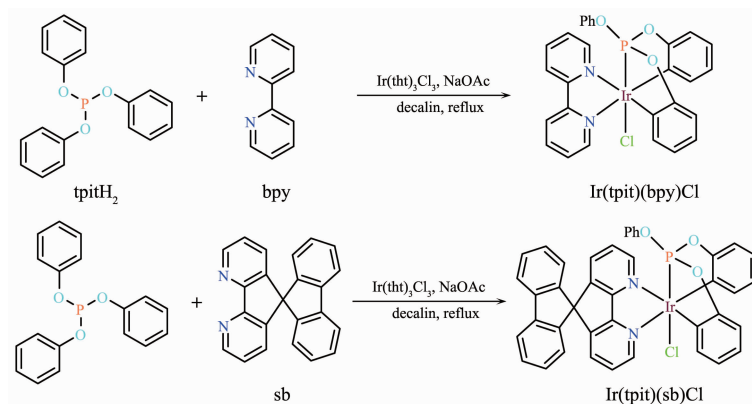
* $w=1/[\sigma^2(F_o^2)+(0.057\ 5P)^2+31.626\ 1P]$, $P=(F_o^2+2F_c^2)/3$.

2 Results and discussion

2.1 Synthesis and characterization

The synthesis route of iridium complex Ir(tpit)(sb)Cl is shown in Scheme 1. The reaction was completed with one-pot method. The coordinated water in raw material $\text{IrCl}_3 \cdot 3\text{H}_2\text{O}$ was replaced by tetrahydrothiophene leading to the increase of oil solubility, enabling the reaction to be carried out in the organic

solvent. The coordination reaction was propitious due to the boiling point of decalin is as high as 187 $^\circ\text{C}$ and it didn't contain active hydrogen disturbing coordination reaction. As an alkali, sodium acetate was able to promote the dehydrogenation process of bicyclic metallization. In combination with the above conditions, the yield of the target iridium complex was achieved to 53% by one-pot reaction. The number of hydrogen in the NMR spectrum of the product was

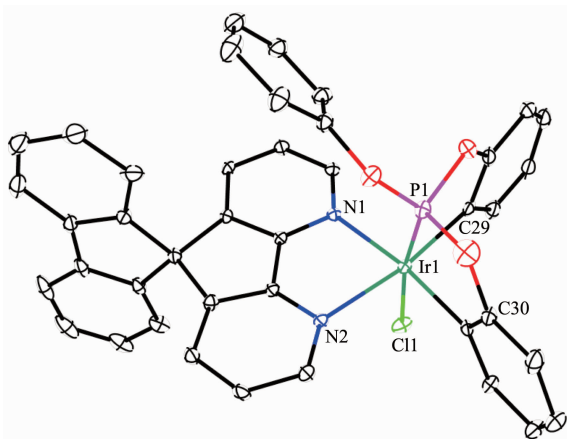


Scheme 1 Synthetic route of iridium complexes

consistent with the theoretical value. Only a single peak signal at δ 113.5 appeared in the phosphorus spectrum, indicating that only one phosphorus ligand participated in the coordination. The charge/mass ratio of the main peak of the HRMS was 819.139 0, which was consistent with the molecular weight (819.138 9) of the target product with dechlorination. All three points above show that the correct target product was obtained.

It should be mentioned that the crystal was only used for the single-crystal structure testing, and dichloromethane-free compounds purified by chromatography on the silica gel column were used for the rest characterization.

The structure of single-crystal is shown in Fig.1. The figure shows a distorted octahedral configuration with the iridium atomic coordination center. The iridium atom coordinates with the phosphite ligand, a sb ligand and a chlorine atom. The phosphorus atom



H atoms and solvent molecules are omitted for clarity;

Selected bond lengths (nm) and angles:

Ir1-C30 0.204 7(8), Ir1-C29 0.205 5(8), Ir1-P1 0.213 4(2),
Ir1-N1 0.219 5(6), Ir1-N2 0.221 3(6), Ir1-Cl1 0.244 6(3),
C30-Ir1-C29 97.0(3)°, C30-Ir1-P1 80.5(3)°,
C29-Ir1-P1 80.7(3)°, C30-Ir1-N1 172.2(3)°,
C29-Ir1-N1 90.7(3)°, P1-Ir1-N1 101.85(18)°,
C30-Ir1-N2 91.7(3)°, C29-Ir1-N2 171.0(3)°,
P1-Ir1-N2 98.31(18)°, N1-Ir1-N2 80.7(2)°,
C30-Ir1-Cl1 93.8(3)°, C29-Ir1-Cl1 94.2(3)°,
P1-Ir1-Cl1 171.77(9)°, N1-Ir1-Cl1 84.58(17)°,
N2-Ir1-Cl1 87.72(18)°

Fig.1 Perspective view of complex Ir(tpit)(sb)Cl with selected displacement ellipsoids drawn at 10% probability level

in the phosphite ester ligand and two benzene rings participate in the coordination in a facial configuration. Because of the molecular limitations of these two cyclometallated benzene rings, phosphorus atoms tilt toward them. The dipyrindine in ligand sb is orthogonal to the two cyclometallated benzene rings, and the spirofluorene in ligand sb is orthogonal to dipyrindine. Therefore, π - π accumulation of uncoordinated benzene rings in phosphite ester with dipyrindine is impeded, which is different from the structure of the reference complex Ir(tpit)(bpy)Cl. It is obvious that Ir(tpit)(bpy)Cl contains intramolecular π - π accumulation, leading to significantly decrease of rotary vibration for uncoordinated benzene rings^[6,8]. The chlorine in the para-position of phosphorus atom neutralizes the surplus positive charge of iridium atoms and lead to electric neutrality of iridium complex. The bond length of Ir-C is 0.204 7 and 0.205 5 nm, the bond length of Ir-N is 0.219 5 and 0.221 3 nm, the bond length of Ir-P is 0.213 4 nm, and the bond length of Ir-Cl is 0.244 6 nm. All these bond lengths are within the bond length range of similar complexes reported in the literature^[6,8-9].

To evaluate the thermophysical properties of complexes, the thermogravimetry analysis (TGA) studies were performed (Fig.2). All these complexes exhibited very good thermal stability. The 5% weight loss temperature (T_d) of complexes Ir(tpit)(bpy)Cl and Ir(tpit)(sb)Cl are 348 and 274 °C, respectively. The higher T_d of Ir(tpit)(bpy)Cl may be attributed to the existence of intramolecular π - π accumulation. The

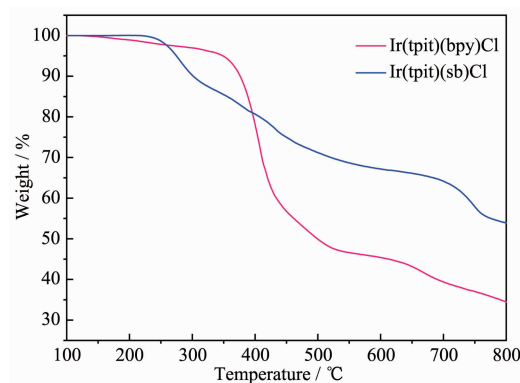


Fig.2 Thermal gravimetric curves of as-prepared iridium(III) complexes

good thermal stability is very advantageous for the preparation of evaporation OLED devices.

2.2 UV-Vis absorption and photoluminescence properties

The UV-Vis spectra of the iridium complexes in CH_2Cl_2 ($10 \mu\text{mol} \cdot \text{L}^{-1}$) and the photoluminescence spectra in PMMA (1%) are shown in Fig.3(a). It can be seen from the figure that the UV-Vis spectra are able to divided into two regions. The first region is the strong bands below 370 nm ($\varepsilon > 4 \times 10^4 \text{ L} \cdot \text{mol}^{-1} \cdot \text{cm}^{-1}$), which is caused by the ligand-centered (LC) $\pi-\pi^*$ transition. The second area at a lower energy region of more than 370 nm absorption bands ($\varepsilon > 1.0 \times 10^4 \text{ L} \cdot \text{mol}^{-1} \cdot \text{cm}^{-1}$) can be attributed to metal-to-ligand charge transfer (MLCT) transitions. Compared with Ir(tpit)(bpy)Cl, the absorption band of Ir(tpit)(sb)Cl in the first area near 330 nm contains one more absorption peak obviously, which can be attributed to the $\pi-\pi^*$ transition absorptions of fluorene groups in sb ligands.

As can be seen from the emission spectra of complexes (Fig.3(a)), the maximum wavelengths of complexes Ir(tpit)(sb)Cl and Ir(tpit)(bpy)Cl are 512 and 520 nm, respectively, in the green region, and the two peaks show the same shape. The blue shift of

emission wavelength for Ir(tpit)(sb)Cl is mainly due to the fact that the LUMO levels of such complexes mainly distribute in pyridine ligands^[6], and spiro-fluorene groups are electron-donating groups so that LUMO energy levels of materials are raised, which can broaden the energy gap and lead to blue shift of wavelengths. In order to reduce luminescence quenching of phosphorescent materials induced by oxygen, complexes were doped in PMMA film with 1% mass concentration. The luminescent life (Fig.2(b) and Table 2) of Ir(tpit)(sb)Cl (1.12 μs) was shorter than that of Ir(tpit)(bpy)Cl (1.60 μs). And its quantum efficiency was 30%, which was far lower than that of Ir(tpit)(bpy)Cl (94%). Based on the above information, the calculated radiation decay rates of Ir(tpit)(sb)Cl and Ir(tpit)(bpy)Cl are 2.7×10^5 and $5.9 \times 10^5 \text{ s}^{-1}$, respectively, and the non-radiation decay rates are 6.3×10^5 and $3.8 \times 10^4 \text{ s}^{-1}$, respectively. It can be found that the radioactive decay rate of Ir(tpit)(bpy)Cl is more than twice as much as that of Ir(tpit)(sb)Cl, while the non-radioactive decay rate of Ir(tpit)(bpy)Cl lowers more than one order of magnitude, indicating that $\pi-\pi$ stacking plays a major role in reducing the non-radioactive transition rate.

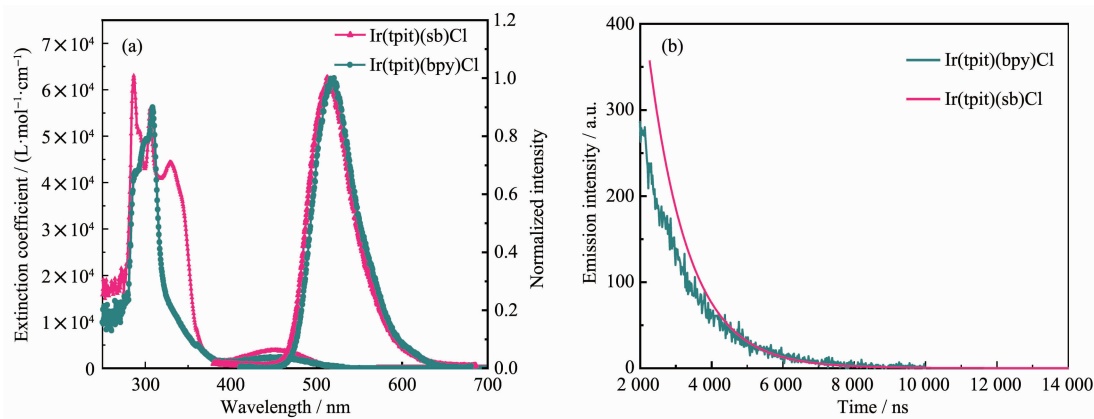


Fig.3 UV-Vis absorption, photoluminescence spectra (a, in CH_2Cl_2) and emission decay curves (b, in PMMA) of iridium(III) complexes

Table 2 Photophysical properties for the iridium complexes

Complex	$\lambda_{\text{max}}^a / \text{nm}$	$\eta^a / \%$	$\tau^a / \mu\text{s}$	$E_{\text{HOMO}}^b / \text{eV}$	$E_{\text{LUMO}}^c / \text{eV}$	$E_{\text{gap}} / \text{eV}$
Ir(tpit)(bpy)Cl	520	94	1.60	-5.72	-3.41	2.31
Ir(tpit)(sb)Cl	512	30	1.12	-5.73	-3.39	2.34

^a Photoluminescence spectra, lifetime and quantum yields were recorded in PMMA at a mass concentration of 1%; ^b $E_{\text{HOMO}} = -4.8 - E_{1/2\text{ox}}$, oxidation potentials $E_{1/2\text{ox}} / \text{mV} = (E_{\text{pa}} + E_{\text{pc}}) / 2$, where E_{pa} and E_{pc} are the anodic and cathodic peak potentials referenced to the Fc^+/Fc couple in CH_2Cl_2 ; ^c LUMO levels $E_{\text{LUMO}} = E_{\text{HOMO}} + E_{\text{gap}}$, where E_{gap} was estimated from the absorption edge.

2.3 Electrochemical properties

The electrochemical properties of iridium complexes were tested by cyclic voltammetry (Fig.4). The oxidation potential of Ir(tpit)(bpy)Cl was 915 mV (vs Fc⁺/Fc). The oxidation potential of Ir(tpit)(sb)Cl was 928 mV, higher than that of Ir(tpit)(bpy)Cl. Thus, the frontier orbital energy levels of complexes were calculated (Table 2). The HOMO energy levels of Ir(tpit)(bpy)Cl and Ir(tpit)(sb)Cl were -5.72 and -5.73 eV, respectively, indicating that instead of ppy, sb ligand can stabilize the HOMO level of complex. According to the ultraviolet absorption edge, the energy gaps of Ir(tpit)(bpy)Cl and Ir(tpit)(sb)Cl were 2.31 and 2.34 eV, respectively, showing an increasing trend, which is consistent with blue shift of luminescence wavelength. The LUMO levels of Ir(tpit)(bpy)Cl and Ir(tpit)(sb)Cl were -3.41 and -3.39 eV, respectively. The higher LUMO level of Ir(tpit)(sb)Cl is caused by

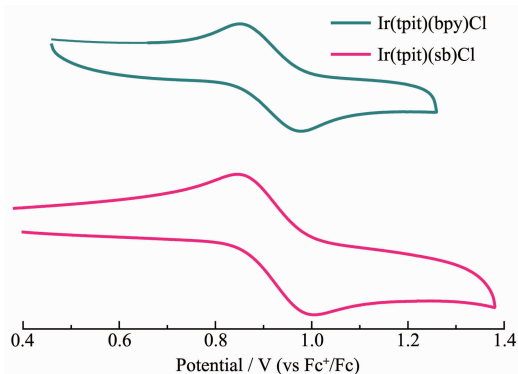


Fig.4 Cyclic voltammetry curves of as-prepared iridium complexes in CH₂Cl₂

the spirofluorene groups which can increase the LUMO level of the complex, proving the blue shift of the luminescence wavelength.

2.4 Electrophosphorescent properties

The electroluminescent devices doped with these iridium complexes were prepared by evaporation method to evaluate their practical application value. The device structure is ITO/TAPC (10 nm)/TCTA (35 nm)/mCP: complex (20 nm)/TmPyPB (50 nm)/Liq (1 nm)/Al (120 nm). Schematic diagram of device structure and energy levels of compounds are shown in Fig.5. Di-(4-(*N,N*-ditolyl-amino)-phenyl) cyclohexane (TAPC) acts as hole injection and hole transport material, and *N,N,N*-tris(4-(9-carbazolyl)phenyl)amine (TCTA) and 1,3,5-tri((3-pyridyl)-phen-3-yl)benzene (TmPyPB) are electron blocking material and electron transport material, respectively. 8-Hydroxyquinolinola (Liq) and aluminum (Al) are used as electron injection transport material and cathode, respectively. The emitting layer is a blend of 1,3-bis(*N*-carbazolyl)benzene (mCP) as the host material and Ir complexes as the dopant with 5%(*w/w*) of Ir(tpit)(bpy)Cl and 8%(*w/w*) of Ir(tpit)(sb)Cl, respectively.

The electroluminescent characteristics and associated data of devices are shown in Fig.6 and Table 3. As shown in Fig.6(a), the maximum wavelengths of Ir(tpit)(bpy)Cl (device **A**) and Ir(tpit)(sb)Cl (device **B**) were at 532 and 520 nm, respectively. Compared with the spectra of complexes in PMMA, these spectra

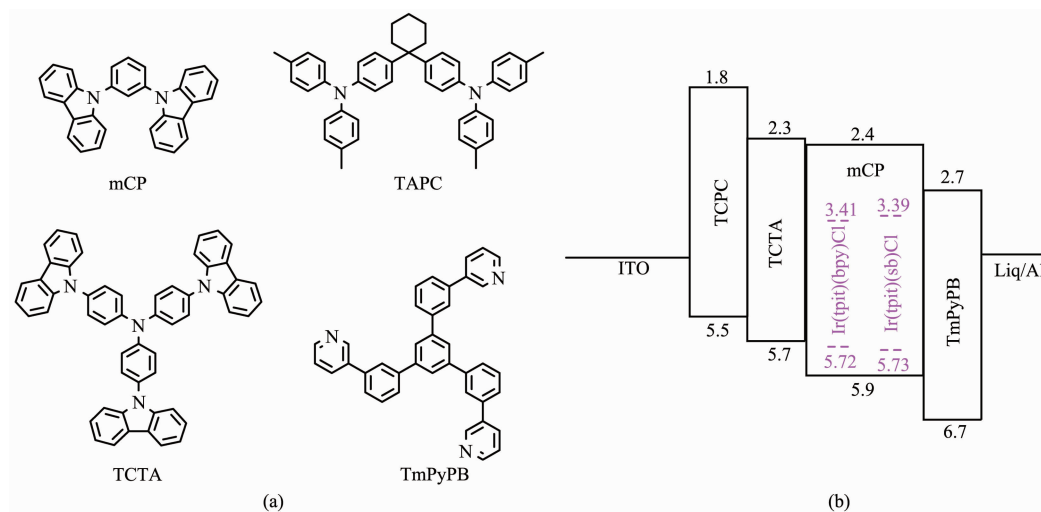


Fig.5 Structural drawing of the materials (a) and energy level diagrams of OLEDs (b)

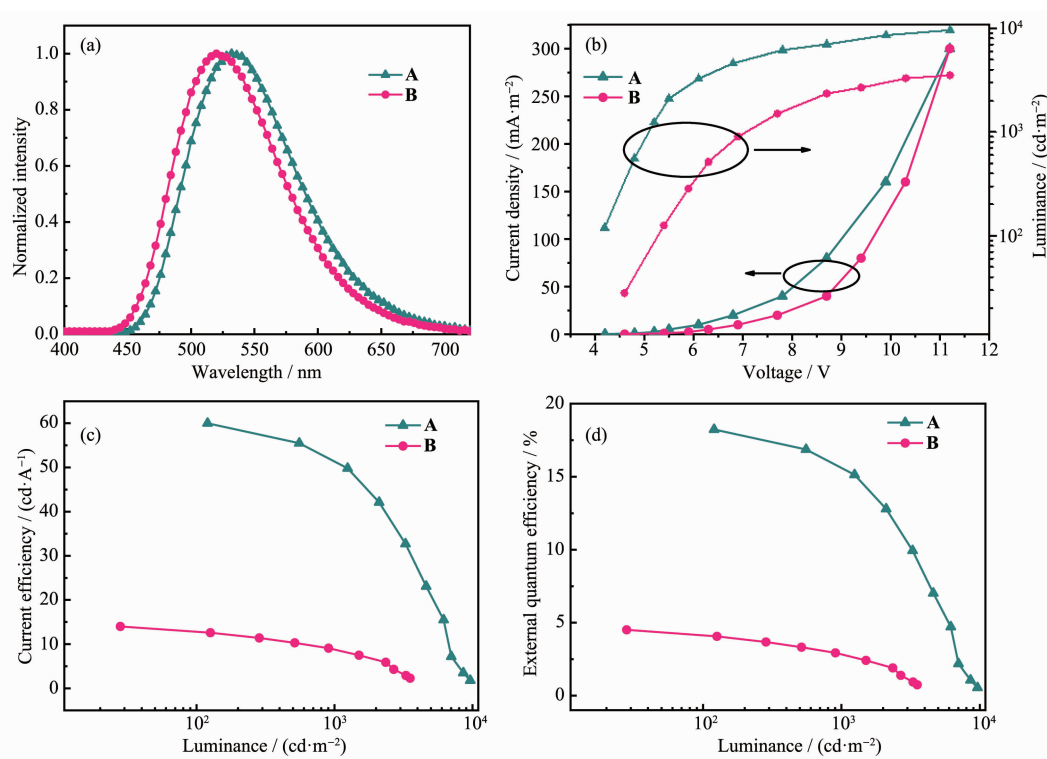


Fig.6 Electroluminescent characteristics and associated data of devices **A** and **B**: (a) EL spectra of all devices; (b) Current density-voltage-luminance (J - V - L) characteristics; (c) Luminance efficiencies vs luminance curves; (d) External quantum efficiency vs luminance curves

Table 3 Summary of device luminescence and efficiency data

Device (Dopant)	$\lambda_{\text{EL,max}}$ / nm	Turn-on voltage / V	Brightness / ($\text{cd} \cdot \text{m}^{-2}$)	Current efficiency / ($\text{cd} \cdot \text{A}^{-1}$)	EQE / %	CIE coordinates (x, y)
A (Ir(tpit)(bpy)Cl)	532	3.6	9 641	60	18.2	0.34, 0.57
B (Ir(tpit)(sb)Cl)	520	4.5	3 531	14	4.6	0.30, 0.55

showed red shift by 12 nm and 8 nm, which is caused by the aggregation effect induced by increase of the concentration of complexes. The space steric hindrance of spirobifluorene can reduce intermolecular aggregation, leading to smaller red shift of Ir(tpit)(sb)Cl. There was no additional peak of the host material in the spectrum, indicating that the energy of it is transmitted to the guests effectively. The turn on voltage of device **A** was about 3.6 V (Fig.6(b)), the luminance increases with the voltage and a maximum luminance of $9\,641\text{ cd} \cdot \text{m}^{-2}$ at 11 V was achieved. In addition, the efficiencies of devices **A** and **B** are revealed in Fig.6(c,d). A maximum current efficiency of $60\text{ cd} \cdot \text{A}^{-1}$ and external quantum efficiency of 18.2% were successfully achieved for device **A** together with CIE of (0.34, 0.57). Device **B** required a higher turn

on voltage of 4.5 V with the maximum brightness of $3\,531\text{ cd} \cdot \text{m}^{-2}$, a maximum current efficiency of $14\text{ cd} \cdot \text{A}^{-1}$ and external quantum efficiency of 4.6% along with the CIE coordinate of (0.30, 0.55). And the external quantum efficiencies of devices are consistent with that of photoluminescence. The efficiency of device **B** was about 25% of that of device **A**, which is mainly caused by the low photoluminescence quantum efficiency resulting from the flexible groups in Ir(tpit)(sb)Cl and lack of intramolecular π - π accumulation.

3 Conclusions

In this paper, a new iridium complex Ir(tpit)(sb)Cl (tpitH₂=triphenyl phosphite) was synthesized by steric ligand 4,5-diaza-9,9-spirobifluorene (sb), and it was compared with the similar complex Ir(tpit)(bpy)Cl

(bpy=2,2'-bipyridine). Crystal structure analysis shows that the spirofluorene groups destroyed the intramolecular π - π accumulation of the complex, leading to blue shift of spectra and decrease of luminescent efficiencies. As for the electroluminescent devices, the maximum current efficiency and external quantum efficiency of complex Ir(tpit)(bpy)Cl were $60 \text{ cd} \cdot \text{A}^{-1}$ and 18.2%, respectively, while the complex Ir(tpit)(sb)Cl achieved lower efficiencies (maximum current efficiency of $14 \text{ cd} \cdot \text{A}^{-1}$ and maximum external quantum efficiency of 4.6%). It means that the intramolecular π - π accumulation plays an important role in reducing the luminescence quenching of the flexible groups. Based on this phenomenon, it is expected to design luminescent materials of iridium complexes with high luminescence performance and aggregation-induced luminescent activity.

Acknowledgements: The authors acknowledge financial support from the National Natural Science Foundation of China (Grant No.21572001).

References:

- [1] Tang C W, Van Slyke S A. *Appl. Phys. Lett.*, **1987**,**51**(12): 913-915
- [2] (a)Tang Y Z, Yu Y M, Tan Y H, et al. *Dalton Trans.*, **2013**, **42**:10106-10111
(b)Tan Y H, Wu J J, Zhou H Y, et al. *CrystEngComm*, **2012**, **14**:8117-8123
(c)Tan Y H, Yang L F, Cao M L, et al. *CrystEngComm*, **2011**,**13**:4512-4518
(d)Tan Y H, Wu J S, Yang C S, et al. *Inorg. Chim. Acta*, **2013**,**399**:45-49
(e)Tang Y Z, Zhou M, Huang J, et al. *Inorg. Chem.*, **2013**, **52**:1679-1681
(f)Tang Y Z, Xiong J B, Gao J X, et al. *Inorg. Chem.*, **2015**, **54**:5462-5466
- [3] Chi Y, Tong B H, Chou P T, et al. *Coord. Chem. Rev.*, **2014**, **281**:1-25
- [4] Chi Y, Chang T K, Ganesan P, et al. *Coord. Chem. Rev.*, **2017**,**346**:91-100
- [5] Lin C H, Chang Y Y, Hung J Y, et al. *Angew. Chem. Int. Ed.*, **2011**,**50**:3182-3186
- [6] Chang Y Y, Hung J Y, Chi Y, et al. *Inorg. Chem.*, **2011**,**50**: 5075-5084
- [7] Lin C H, Lin C Y, Hung J Y, et al. *Inorg. Chem.*, **2012**,**51**: 1785-1795
- [8] WEI Liang-Chen(魏良晨), HU Wei-Kang(胡伟康), ZHOU Shi-Xiong(周世雄), et al. *Chem. J. Chinese Universities*(高等学校化学学报), **2018**,**39**:1371-1377
- [9] Mei Q Y, Shu J, Zhou S X, et al. *Inorg. Chem. Commun.*, **2018**,**98**:62-67
- [10]Chen H F, Hung W Y, Chen S W, et al. *Inorg. Chem.*, **2012**,**51**:12114-12121
- [11]Bolink H J, Coronado E, Costa R D, et al. *Adv. Mater.*, **2008**,**20**:3910-3913
- [12]Costa R D, Orti E, Bolink H J, et al. *J. Am. Chem. Soc.*, **2010**,**132**:5978-5980
- [13]Tordera D, Meier S, Lenes M, et al. *Adv. Mater.*, **2012**,**24**: 897-900
- [14]He L, Ma D, Duan L, et al. *Inorg. Chem.*, **2012**,**51**:4502-4510
- [15]Congrave D G, Hsu Y T, Batsanov A S, et al. *Dalton Trans.*, **2018**,**47**:2086-2098
- [16]Chi C C, Chiang C L, Liu S W, et al. *J. Mater. Chem.*, **2009**, **19**:5561-5571
- [17]Wong K T, Chen R T, Fang F C, et al. *Org. Lett.*, **2005**,**7**: 1979-1982
- [18]Wang Y C, Xie Y Y, Qu H E, et al. *J. Org. Chem.*, **2014**, **79**:4463-4469
- [19]TONG Bi-Hai(童碧海), LIU Yuan-Yuan(刘远远), ZHANG Man(张曼), et al. *Chinese J. Inorg. Chem.*(无机化学学报), **2014**,**30**:1174-1178
- [20]Wang S M, Zhang J Y, Hou Y H, et al. *J. Mater. Chem.*, **2011**,**21**:7559-7561
- [21]Hong M, Zhang K, Li Y Z, et al. *Polyhedron*, **2009**,**28**:445-452
- [22]Su H C, Fang F C, Hwu T Y, et al. *Adv. Funct. Mater.*, **2017**,**17**:1019-1027
- [23]Su H C, Wu C C. *Appl. Phys. Lett.*, **2006**,**89**:261118
- [24]Chen H F, Wong K T, Liu Y H, et al. *J. Mater. Chem.*, **2011**,**21**:768-774
- [25]Su H C, Chen H F, Fang F C, et al. *J. Am. Chem. Soc.*, **2008**,**130**:3413-3419
- [26]Sheldrick G M. *SADABS*, University of Göttingen, Germany, **1996**.
- [27]Sheldrick G M. *Shelxtl Software Reference Manual*, Ver. 5.1, Bruker AXS Inc., Madison, Wisconsin (USA), **1997**.